Progressive Point Cloud Upsampling via Differentiable Rendering

Pingping Zhang, Xu Wang, *Member, IEEE,* Lin Ma, *Member, IEEE,* Shiqi Wang, *Member, IEEE,* Sam Kwong, *Fellow, IEEE,* Jianmin Jiang

***Abstract*—In this paper, we propose one novel progressive point cloud upsampling framework to tackle the non-uniform distribution issue during the point cloud upsampling process. Specifically, we design an Up-UNet feature expansion module which is capable of learning the local and global point features via a down-feature operator and an up-feature operator, respectively, to alleviate the non-uniform distribution issue and remove the outliers. Moreover, we design a hybrid loss function considering both the multi-scale reconstruction loss and the rendering loss. The multi-scale reconstruction loss enables each upsampling module to generate a denser point cloud, while the rendering loss via point-based differentiable rendering ensures that the proposed model preserves the point cloud structures. Extensive experimental results demonstrate that our proposed model achieves state-of-the-art performance in terms of both qualitative and quantitative evaluations. Github: https://github.com/ppingzhang/PPU.git**

***Index Terms*—Point cloud upsampling, point-based differential rendering, feature expansion unit**

I. INTRODUCTION

RECENT years have witnessed dramatically increased interest in point cloud based applications. However, due to the hardware and computational constraints, 3D sensors such as LiDAR often produce sparse, noisy and non-uniformly distributed raw point cloud data [1], [2], [3], [4]. Since the performance of 3D vision tasks is highly influenced by the integrity of the input point cloud data, improvement of the raw data quality via point cloud upsampling becomes an essential step to enable the downstream applications, such as 3D object classification [5], semantic segmentation [6], and shape reconstruction [7], [8], [9], [10], [11].

This work was supported in part by the National Natural Science Foundation of China (Grant 61871270 and 61620106008), in part by the Shenzhen Natural Science Foundation under Grants JCYJ20200109110410133 and 20200812110350001, in part by the National Engineering Laboratory for Big Data System Computing Technology of China. *(Corresponding Author: Dr. Xu Wang)*

Pingping Zhang is with the College of Computer Science and Software Engineering, Shenzhen University, China, and also with the Department of Computer Science, City University of Hong Kong, Kowloon, Hong Kong. Email: (ppingyes@gmail.com).

Xu Wang and Jianmin Jiang are with the College of Computer Science and Software Engineering, Shenzhen University, China, and also with Guangdong Laboratory of Artificial Intelligence and Digital Economy (SZ), Shenzhen University, Shenzhen, 518060, China. Email: (wangxu@szu.edu.cn, jianmin.jiang@szu.edu.cn).

Lin Ma is with Meituan, China. Email: (forest.linma@gmail.com).

Shiqi Wang and Sam Kwong are with the Department of Computer Science, City University of Hong Kong, Kowloon, Hong Kong. Email: (shiqwang@cityu.edu.hk; cssamk@cityu.edu.hk).

Compared with the traditional 2D image super-resolution task, the point cloud upsampling task is more challenging. First, unlike the 2D image with a regular sampling grid [12], the raw point cloud is irregular, sparse, noisy and non-uniform. Thus, the point cloud upsampling task aims to not only produce a denser version, but also remove noise, protect the structure and thereby generate a dense and uniformly distributed point cloud. Second, the objectives of the point cloud upsampling task are supposed to be application dependent [5], [13]. As a point cloud set is only an intermediate representation of the 3D scene, the generated points should be informative and uniform to assist other applications, such as surface reconstruction and view synthesis.

Numerous efforts [14], [15], [16], [9], [10], [17], [18] have been devoted to investigating point cloud upsampling techniques to ensure the consistency and integrity of point cloud data. The earlier works focused on reconstructing a piece-wise smooth representation of the original shape, and specialized priors have been incorporated to address the challenges from data imperfections [19], [20], [21]. However, these priors may not always be appropriate, and in practice, certain shapes may fail to adhere to these priors. More recently, inspired by the success of point-based deep learning [22], deep learning-based point cloud upsampling techniques [9], [10] have attracted growing attention. Many learning-based works attempt to reconstruct uniformly distributed points, which are located close to underlying surfaces. For example, Yu *et al.* [9] proposed a repulsion loss in the PU-Net to make points more uniformly. Li *et al.* [10] proposed a uniform loss to generate point clouds with uniform distribution. However, these models largely ignore the local quality of the reconstructed surface. Since point clouds are unordered, existing loss functions can only measure the global quality of dense point cloud data but cannot preserve the local quality of reconstructed surfaces. Moreover, most models were designed for a fixed upsampling ratio. To upsample with varying scales, they need to train multiple models with pre-defined ratios. Some models need to call numerous times because they break upsampling into multiple small upsampling. For example, a $4\times$-upsampling operation needs to be broken into two $2\times$ steps, so this model needs to be called twice. These methods increase the model complexity, as well as the training and testing time.

To resolve the challenges, we propose a progressive point cloud upsampling framework via the point-based differentiable rendering, which tackles the non-uniform distribution issue of the point cloud. Specifically, the proposed upsampling framework consists of a contextual representation (CR) module and a number of cascaded upsampling modules with shared parameters. To support the progressively upsampling, our model shares different resolution information both inside and between upsampling modules, and each of them produces a denser point cloud to achieve multi-scale upsampling. Inspired by the concept of the point-based differentiable rendering [23], a rendering loss is proposed to enforce the network to learn the underlying geometry of a latent target object via measuring the fidelity of synthesized images under different camera poses. Accordingly, the error back propagates through the differentiable renderer, so the network is capable of learning the structure preserved features. We conduct extensive experiments on a sparse, noisy and incomplete dataset to demonstrate the effectiveness of our approach, aiming to generate high quality dense and complete point clouds. As a result, our approach leads to outstanding performance for the final point cloud upsampling results surpassing the state-of-the-art (SOTA) methods. Moreover, ablation studies and experimental analyses demonstrate the intermediate benefits of our method.

In summary, the main contributions of this paper lie in the following three folds.

1) We propose a flexible framework that can upsample point cloud progressively to support multi-scale upsampling. The proposed Up-UNet feature expansion unit enables the model to learn global point features, remove the outliers and alleviate the non-uniform issue.
2) We design a hybrid loss function considering both multi-scale reconstruction loss and rendering loss. The multi-scale reconstruction loss enables each upsampling unit to output a denser point cloud, while the rendering loss via the point-based differentiable rendering forces the model to learn the structure preserved features.
3) Extensive experiments and analyses verify the effectiveness of our approach on different point cloud tasks. The proposed approach improves the quality of reconstructed point cloud and outperforms the SOTA methods.

II. Related Work

A. Point Cloud Processing

There are three typical point cloud processing tasks: point cloud upsampling, point cloud denoising and point cloud completion. From the aspect of optimization-based methods [14], [24], [25], [13], most of them consider various shape priors to constrain the geometry reconstruction. Alexa *et al.* [24] provided a framework to approximate a smooth manifold surface defined by a set of points and resampled the surface to generate an adequate representation of the surface. Lipman *et al.* [25] introduced a Locally Optimal Projection for surface approximation from point cloud data. Huang *et al.* [13] modified and extended the LOP operator to produce a clean and uniformly distributed point set endowed with reliable normals. These traditional point cloud processing methods mostly consider surface reconstruction. Due to the excellent performance of deep learning, these traditional tasks have a better outcome under this method. To generate uniform dense point clouds, Yu *et al.* [26] presented EC-Net, which is the first edge-aware network for consolidating point clouds. PU-Net [9], PU-GAN [10] and MPU [16] can remove outliers and generate dense point clouds simultaneously. PUGeo-Net [11] can compute normals for the original and generated point clouds to improve the quality of the surface reconstruction. To improve the surface approximation via point set upsampling, Lin *et al.* [27] proposed CAD-PU to realize the curvature-adaptive feature expansion.

Most of the upsampling models can not process point clouds with large holes [26], since the point cloud structure was destroyed and these models can not extract the critical structure effectively. In this context, point cloud upsampling tasks share the same aim as point cloud completion tasks, as they need to achieve point cloud inpainting to guarantee the completion of the whole structure and obtain a uniform and dense point cloud [28]. As such, point cloud completion is also a popular topic in 3D reconstruction. PF-Net [29] generated the target point cloud with both rich semantic profiles and detailed characters while retaining the existing contour. These models can achieve point cloud inpainting to guarantee the completion of the whole structure. Nevertheless, it can not indicate that their models can remove the outliers and generate a dense point cloud uniformly. PCN [30] generated a dense point cloud in a coarse-to-fine fashion on raw point clouds without voxelization. ECG [31] can complete the point cloud by two stages, which are the coarse and fine stages. Likewise, Wang *et al.* proposed a cascaded refinement network together with a coarse-to-fine strategy to synthesize the detailed object shapes [32]. Their model considered the local details of partial inputs with the global shape information together. Analogously, our model can achieve the point cloud reconstruction progressively via multiscale fine-tuning. Benefited from the special model design and the hybrid loss, our proposed model can complete various point cloud tasks, *e.g.*, upsampling, denoising and completion.

B. Point-based Functional Module

Existing point cloud upsampling models [9], [10], [16] design point-based functional modules by employing the common architectures such as ResNet [33], DenseNet [34] and UNet [35] as backbones. Owing to the limitation of model structure, these models can only process noisy point clouds and conduct dense point clouds under the same structure, but they can not guarantee the good quality of the point cloud upsampling task with serious noise. For example, PU-Net [9] and PU-GAN [10] can process the point cloud with slight noise. Our proposed Up-UNet feature expansion module consists of an up-feature operator and a down-feature operator, which combine the benefits of existing point-based functional modules to process the noisy point clouds well.

A popular and simple up-feature is to duplicate the feature multiple times. However, this strategy could not protect the point structure information, such that PU-GAN and MPU introduce the grid information to guide point cloud upsampling. The down-sampling layer, the inverse process of upsampling, can extract key points and corresponding features. The traditional methods, such as farthest point sampling and Poisson

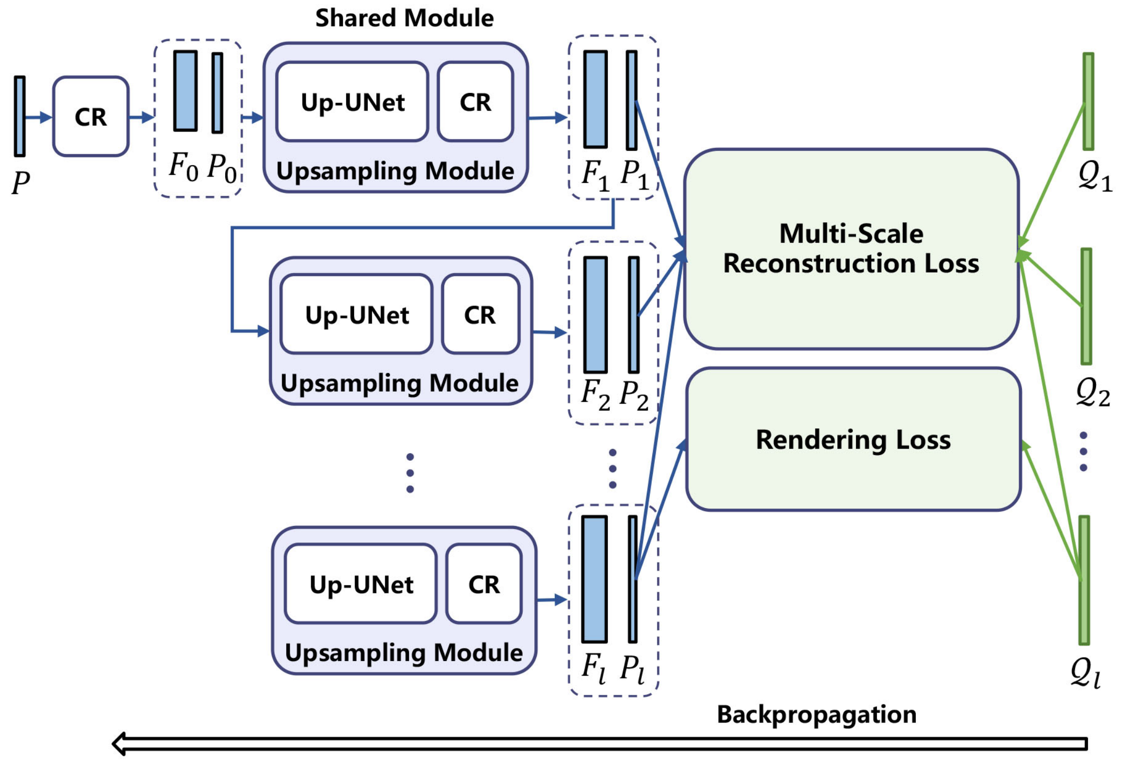

Fig. 1. The architecture of our proposed model. The shared upsampling module consisting of an Up-UNet and a CR module is cycled multiple times. The loss function mainly is composed of the multi-scale reconstruction loss and the rendering loss. Due to the point-based differentiable rendering, the error can be backpropagated.

disk sampling, have been widely used for decades. Inspired by the success of PointNet [36] on classification, many key point extraction methods were studied in recent years. The PointNet++ [22] captures both local geometry contexts via a hierarchical feature learning architecture. These models only deal with a single function and can not effectively combine. Our proposed Up-UNet, based on the UNet, learns the global and local features via an up-feature operator and a down-feature operator, respectively, to effectively alleviate the non-uniform distribution issue and remove the outliers.

C. Differentiable Rendering

Renderers are traditionally designed to solve the forward process of image synthesis. Recently, deep learning has been popular in 3D reconstruction tasks [37], [38], [39], [23], [40], [41]. Therefore, various differentiable rendering techniques were introduced to generate rendering images, which also can help 3D model reconstruction via error backpropagation. Existing differentiable renderers can be classified into four categories according to the geometric representation: point-based [23], [42], [43], [40], voxel-based [44], [45], [46], mesh-based [47], [48], [37] and implicit neural function based [49], [50]. Voxel-based methods come with high memory requirements even for relatively coarse geometries. Mesh-based methods exploit the sparseness of the underlying geometry in the 3D space. However, converting into a mesh form is a challenging and error-prone operation. These methods are limited to global and topological changes, and connectivity is not differentiable. More recently, implicit neural functions are popularly applied to represent scenes, as they can achieve a high spatial resolution. However, existing approaches are limited by the low network capacity and inaccurate intersections of camera rays with the scene geometry. Point-based methods directly operate on point samples of the geometry, which is flexible and efficient. In this context, a fast and effective point-based differentiable renderer [23] is adopted to capture rendering images from various camera poses, which contributes to the local geometry reconstruction.

III. Proposed Model

Suppose the captured raw point cloud is denoted as $\mathcal{P} = \left\{\mathbf{p}_i \in \mathbb{R}^d\right\}_{i=1}^{N}$ of N points, where d is the dimension of the input point cloud attributes, *i.e.*, coordinates, color and normal. Here, we only consider the 3D coordinates with d = 3. The point cloud upsampling network aims to generate a denser point cloud $\hat{\mathcal{P}} = \left\{\hat{\mathbf{p}}_i \in \mathbb{R}^d\right\}_{i=1}^{rN}$ with upsampling ratio r from $\mathcal{P}$, by minimizing the reconstruction distance between $\hat{\mathcal{P}}$ and the ground truth (GT) points $\mathcal{Q} = \left\{\mathbf{q}_i \in \mathbb{R}^d\right\}_{i=1}^{rN}$. As shown in Fig. 1, the pipeline of our proposed model consists of a CR module and L cascaded upsampling module with shared parameters. The CR module first transforms the raw point cloud into the feature domain and outputs the aggregated point-wise feature map $\mathcal{F}_0$ and initially reconstructed point cloud $\mathcal{P}_0$. The following upsampling module will progressively process the point cloud $\mathcal{P}_{l-1}$ with the upsampling ratio r_l for the l-th module and output the reconstructed point cloud $\mathcal{P}_l$. When L is set to 1 and the first up-feature operator is withdrawn, it becomes a point cloud completion network. Details of our proposed CR module and Up-UNet feature expansion module are discussed as follows.

A. *Contextual Representation Module*

The proposed CR module aims to extract point features from the noisy input and output the reconstructed points for the next upsampling iteration. Specifically, our proposed CR module consists of feature extraction and coordinate reconstruction operators. We adopt the feature extraction module in [16], which can integrate features across different layers through dense connections. In each dense block, it generates a local neighbourhood which is computed dynamically via feature-based K-Nearest Neighbor (KNN). Then, a chain of densely connected Multilayer Perceptron (MLP) layers refine grouped features, and finally, a max-pooling operator is applied to achieve order-invariance. Accordingly, the coordinate reconstruction operator is capable of extracting long-range and non-local information. The CR module is embedded into the primary stage and the end of each Up-UNet upsampling module. The purpose of the first CR module aims to extract the contextual features F_0, and initially reconstructed points P_0.

B. *Upsampling Module*

As shown in Fig. 1, our proposed upsampling module consists of an Up-UNet feature expansion unit and a CR module. Unlike the official UNet architecture [35], our proposed module firstly upsamples point features via an up-feature operator, which not only extracts the local point features but also adjusts the features according to the neighbouring features via a channel attention operator. Besides, such upsampling module can maintain the order of the input point cloud since the number of features is doubled by duplication. Then, to keep the consistency of the guided point cloud, we split the first N point features from the upsampled features. The first down-feature operator only conducts the sampling operation without changing the number of points, which extracts neighbouring information and builds the relation of closing points. The second down-feature operator performs the real downsampling to extract key points and important point features. Subsequently, the continuous upsampling operations, together with the expansive paths, allow the network to propagate context information to reconstruct a dense point cloud.

For progressive upsampling, a CR module is stacked after an Up-UNet feature expansion unit for the coordinate reconstruction of the upsampled point cloud. Since all the Up-UNet and CR units share the same parameters, our proposed upsampling module can handle point clouds with various upsampling ratios. Details of the up-feature operator and the down-feature operator are discussed as follows.

1) Up-feature Operator: The up-sampling operator is indispensable in the point cloud upsampling task. A common and simple way is to duplicate the feature multiple times. However,

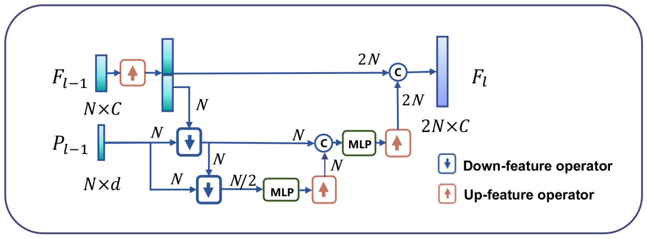

(a) Up-UNet

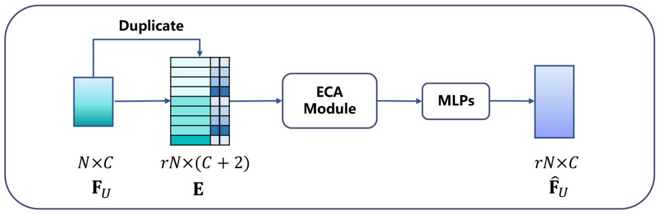

(b) Up-feature operator

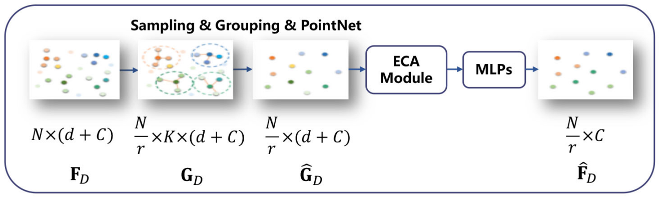

(c) Down-feature operator

Fig. 2. Figure (a) is the case of $2\times$ upsampling. Operators in our proposed Up-UNet feature expansion modules: (a) Up-UNet; (b) Up-feature operator; (c) Down-feature operator.

this way can not protect the point structure information. Therefore, to expand the input point feature $\mathbf{F}_U \in \mathbb{R}^{N\times C}$ for r times, our proposed up-feature operator unfolds the point features based on the 2D grid. As shown in Fig. 2, the 2D grid mechanism in FoldingNet [51] is adopted to generate a unique 2D vector via per feature-map copy. Specifically, the grid position matrix is denoted as $\mathbf{G}_U \in \mathbb{R}^{r\times 2}$. Meanwhile, the expanded feature $\mathbf{E} \in \mathbb{R}^{rN\times(C+2)}$ is generated by duplicating and concatenating input point features and a grid position vector. The j-th node of expanded feature $\mathbf{E}$ is defined as $\mathbf{E}_j = (G_{j\%r}, F_{j/r})$. Based on the folding method, the up-feature operator can increase the variation of point features in the distribution density.

To improve both local channel interaction of point features, we adopt the ECA unit [52] to readjust features via feature aggregation of the nearest neighbouring features. Compared with other attention modules, such as the spatial attention module [53], [54] and the convolutional block attention module [55], the ECA unit can appropriate cross-channel interaction to preserve features and benefits the point feature reconstruction. At the end of the module, a set of MLPs is applied to refine and produce more consistent geometric details for the final expanded point features.

2) Down-feature Operator: The down-feature operator, the inverse process of upsampling, can extract key points and corresponding features. The traditional methods, such as farthest

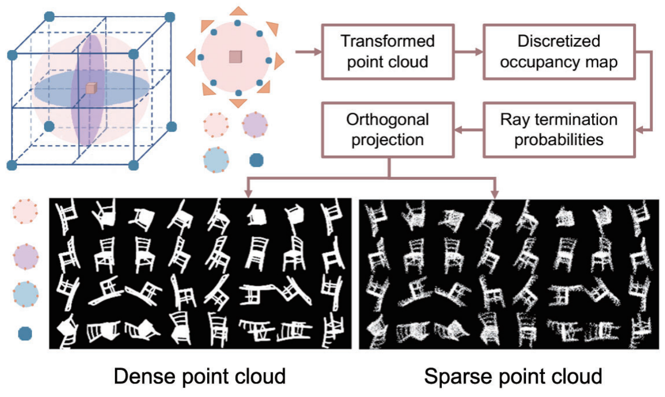

Fig. 3. The first row shows the pipeline of the differentiable point cloud renderer [23]. Points in the cube represent the camera poses. The second row is the rendering results of dense point clouds and its sparse version with 32 camera poses.

point sampling and Poisson disk sampling, are widely used for decades. Inspired by the success of PointNet++ [22], it can capture local geometry contexts via a hierarchical feature learning architecture. Thus, our down-feature operator integrates a similar downsampling policy to extract important point features.

Accordingly, our proposed down-feature operator aims to hierarchically group input point features and progressively abstracts key points features. To extract both local and global salient point features from noisy input point features, we apply the local learning mechanism on the input point features $\mathbf{F}_D$ with the guidance of the input point cloud $\mathcal{P}_D$. Specifically, the proposed local feature extractor comprises three key layers: a sampling layer, a grouping layer and a PointNet layer. The sampling layer initially selects the centroids of local regions following iterative farthest point sampling (FPS) to choose a subset with $\frac{N}{r}$ points and the corresponding point features. Then, the grouping layer constructs a group of local point features $\mathbf{G}_D \in \mathbb{R}^{\frac{N}{r} \times K \times (d+C)}$ by finding K neighbouring points around the centroids. Finally, each local region is abstracted by its centroid and local features via a mini-PointNet, which encodes local region patterns $\mathbf{G}_D$ into feature vectors $\hat{\mathbf{G}}_D \in \mathbb{R}^{\frac{N}{r} \times (d+C)}$. The module can capture point-to-point relations in the local region by using relative coordinates together with point features. Same as the up-feature operator, an ECA module and a set of MLPs are applied to obtain point features $\hat{\mathbf{F}}_D \in \mathbb{R}^{\frac{N}{r} \times C}$.

C. Loss Function

We propose a novel hybrid loss function to train the network for point cloud upsampling. This hybrid loss contains a reconstruction loss and a rendering loss, which can encourage the model to reconstruct detailed point clouds.

Multi-Scale Reconstruction Loss The multi-scale reconstruction loss measures the difference between the output points and the GT points with different resolutions. Point clouds are disordered, such that we employ the Chamfer Distance (CD) [56] as the reconstruction loss, which is invariant to permutations of the points. Specifically, we use the following symmetric CD function, which calculates the average closest distance between the output point cloud $\mathcal{P}_l$ of the l-th upsampling unit and the corresponding GT points $\mathcal{Q}_l$, the downsampled version of the GT points $\mathcal{Q}$. In this context, our model can produce upsampling point clouds with multiple ratios and ensuring the quality of the upsampled point cloud.

$$\begin{aligned}\mathcal{L}_{CD}\left(\mathcal{P}_l, \mathcal{Q}_l\right) = & \frac{1}{|\mathcal{P}_l|} \sum_{\mathbf{p} \in \mathcal{P}_l} \min_{\mathbf{q} \in \mathcal{Q}_l} \|\mathbf{p} - \mathbf{q}\|_2 \\ & + \frac{1}{|\mathcal{Q}_l|} \sum_{\mathbf{q} \in \mathcal{Q}_l} \min_{\mathbf{p} \in \mathcal{P}_l} \|\mathbf{q} - \mathbf{p}\|_2 .\end{aligned} \tag{1}$$

The first term in Eq. (1) focuses on minimizing the distance of output points and the closest GT point, whereas the second term ensures that the GT point cloud is covered by the output point cloud. Finally, we measure the overall reconstruction loss $\mathcal{L}_R$ by merging the reconstruction loss of all the upsampling units,

$$\mathcal{L}_R = \sum_{l=1}^{L} \lambda_l \mathcal{L}_{CD}\left(\mathcal{P}_l, \mathcal{Q}_l\right), \tag{2}$$

where λ_l represents the weight of the l-th upsaming unit.

Rendering Loss. Inspired by the model from Insafutdinov *et al.* [23], we introduce the rendering loss to learn high-fidelity shape models solely from their projections. Instead of learning camera poses, we fix the multiple cameras poses to estimate the rendering views. In this way, our model can reconstruct point clouds by preserving the details.

To ensure the fidelity of the synthesized images rendered from the reconstructed point cloud, we employ the point-based differentiable renderer π as in [23], which projects 3D point cloud data into 2D view images according to the camera pose settings. The pipeline of the point cloud renderer is illustrated in Fig. 3. First, it transforms the 3D coordinate of the raw point cloud into the standard coordinate frame by the projective transformation corresponding to the camera pose. Second, to guarantee the back-propagation of a gradient in the training stage, the discretized point is represented as scaled Gaussian densities to obtain the occupancy map. By introducing the differentiable ray tracing operator, the occupancies are converted into ray termination probabilities. Final, the projected image is obtained by projecting the volume to the plane.

Specifically, given the s-th pose c_s, we obtain raw projected view images $\mathbf{I}_s = \pi(\mathcal{Q}, c_s)$ and reconstructed projected view images $\hat{\mathbf{I}}_s = \pi(\hat{\mathcal{P}}, c_s)$ from the groundtruth $\mathcal{Q}$ and final output $\hat{\mathcal{P}}$, respectively. The rendering loss $\mathcal{L}_v$ is defined as the mean absolute difference of $\hat{I}_s$ and $\hat{I}_s$ for all the camera poses. That is,

$$\mathcal{L}_v = \frac{1}{SWH} \sum_{s=1}^{S} \sum_{x=1}^{W} \sum_{y=1}^{H} |\mathbf{I}_s(x, y) - \hat{\mathbf{I}}_s(x, y)|, \tag{3}$$

where S is the total number of camera poses. In this work, we take 8 camera poses evenly on the projection plane of each rotation axis (x, y, z), and there are 8 camera positions in each diagonal position with a total of 32 camera poses, as shown in Fig. 3. Specifically, three colour planes in Fig. 3

represent different projection planes. The 8 points in the colour planes denote 8 camera positions of rendering images in each row. Compared with the rendering images of the sparse point clouds, the rendering images from the dense point clouds are more clear and have high resolution. The rendering loss combined with multiple local rendering images will enforce the network to reconstruct local features of point clouds.

Hybrid loss Overall, we train our model by minimizing $\mathcal{L}$:

$$\mathcal{L} = \mathcal{L}_R + \alpha \mathcal{L}_v + \beta \|\theta\|^2, \tag{4}$$

where α is the weight of $\mathcal{L}_v$, θ indicates the parameters in our network and β denotes the multiplier of the weight decay.

IV. Experimental Results

In this section, we conduct extensive experiments to evaluate the performance of our proposed model. In the following subsections, we first describe the experimental settings such as datasets, evaluation metrics and implementation details. Details on the performance comparison between the proposed model and the SOTA models are described as follows.

A. Experimental Settings

1) Datasets: To objectively compare the performance of the model, we train and test our model under the dataset provided by PU-GAN [10], which collected 147 3D models from the released datasets of PU-Net [9] and MPU [16], as well as from the Visionair repository [57]. For each point cloud, we randomly crop 200 patches and collect 24,000 patches in total. By default, we set the input number N as 256, the upsampling ratio r as 4. Moreover, we add different degrees $\theta \in \{0.5\%, 1\%, 1.5\%, 2.5\%\}$ of Gaussian noise to evaluate the model's ability of noisy removal. For the point completion task, we also train and test our model from a subset of the Shapenet dataset [58] derived from the dataset in Yuan *et al.* [30]. In our experiments, both input and GT point clouds are sampled 2048 points uniformly. To avoid overfitting in training, we augment the network inputs by random rotation and scaling.

2) Implementation Details: We trained the network with 100 epochs via the Adam algorithm [59]. We set the learning rates as 0.001, and it gradually reduces with the increase of iterations. The batch size is 28, and $\{\lambda_1, \lambda_2\} = \{1.0, 0.3\}$ and both α and β are empirically set as 1.0. Different from MPU, our training only needs one stage. We implemented our network using TensorFlow and trained it on the Tesla V100 GPU.

Our model can adapt to multi-resolution upsampling. Take the $4\times$ model as an example that PU-GAN only achieves the $N \times 4$ upsampling. If PU-GAN requires to realize $2\times$ upsampling, it needs to samples the results of $4\times$ upsampling. Unlike PU-GAN, our model can directly obtain the output of the first Up-UNet module as the result of $2\times$ upsampling, and the second Up-UNet module, as a result of $4\times$ upsampling. If we want to achieve a higher ratio upsampling, we need to carry on the cycle operation on the basis of $4\times$ upsampling because the transformation of $4\times$ feature space is considered in the model training. If our model upsamples points with $16\times$ or higher times, we can get the middle $2\times$, $4\times$, $8\times$ results directly. For other upsampling ratios, we can sample the given number of points from the upsampled points.

3) Evaluation Metrics: For quantitative evaluation, we employ the point-to-surface (P2F) distance, CD, and Hausdorff distance (HD) [60] to evaluate our proposed model against the SOTA methods on point cloud upsampling and denoising. Each ground truth 3D model contains 8192 points, and then we randomly select 2048 points as the testing input. Similarly, we follow the patch-based strategies in PU-GAN, MPU, EC-Net and PU-GAN to extract a local patch with 256 points per seed. Then, after processing, these sub-patches are combined as the final output. For the point completion task, we evaluate our model across 8 classes from the Shapenet dataset [58]. For each class, the CD is employed to evaluate the reconstructed models.

B. Comparisons with the State-of-the-Art Methods

In this subsection, our proposed method is compared with the SOTA methods on different tasks, including point cloud upsampling, denoising and completion.

1) Point Cloud Upsampling: We qualitatively and quantitatively compare our proposed method with three SOTA point cloud upsampling methods, including PU-Net [9], MPU [16], and PU-GAN [10]. We use their public code and retrain their networks on our training dataset. Table I shows the quantitative comparison results, which are the average results in the testing data. Our proposed method achieves the lowest values for all the evaluation metrics. Besides quantitative results, some examples of upsampling results for all the methods are provided in Fig. 4 for four different 3D models ("Horse", "Tiger", "Status" and "Camel"). The first row (Input) shows the input point clouds, and the second row (GT) is the corresponding dense points. We amplify the local point cloud and find that our proposed method has a good performance to deal with complex areas and produces more fine-grained details.

To analyze the influence of the reconstructed point cloud on the synthesized images, we further provide examples of synthesized images for the upsampled 3D point clouds in Fig. 5. It is observed that there are many holes in the synthesized images for methods PU-Net, MPU and PU-GAN, which do not consider the surface reconstruction in their architecture design. The above models can not deal with the complex 3D model with occluded objects or surfaces since the input sparse point clouds do not have complete structures. Our proposed method can learn the structure prior from the training dataset via the constraint of rendering loss.

2) Point Cloud Denoising: To demonstrate the robustness of our proposed model on noise tolerance, we evaluate all pre-trained models on a synthetic dataset with different noisy levels, including 0.5%, 1.0%, 1.5%, and 2.5%, respectively. All the methods are implemented to $4\times$-upsamping the noisy point clouds. Table I shows the comparison results of point cloud upsampling with different noisy levels. It is observed that the performance of all the methods decreases as the noise level increases. As illustrated in Fig. 6, for point clouds with noise level 0.5% , most models can get rid of noise and

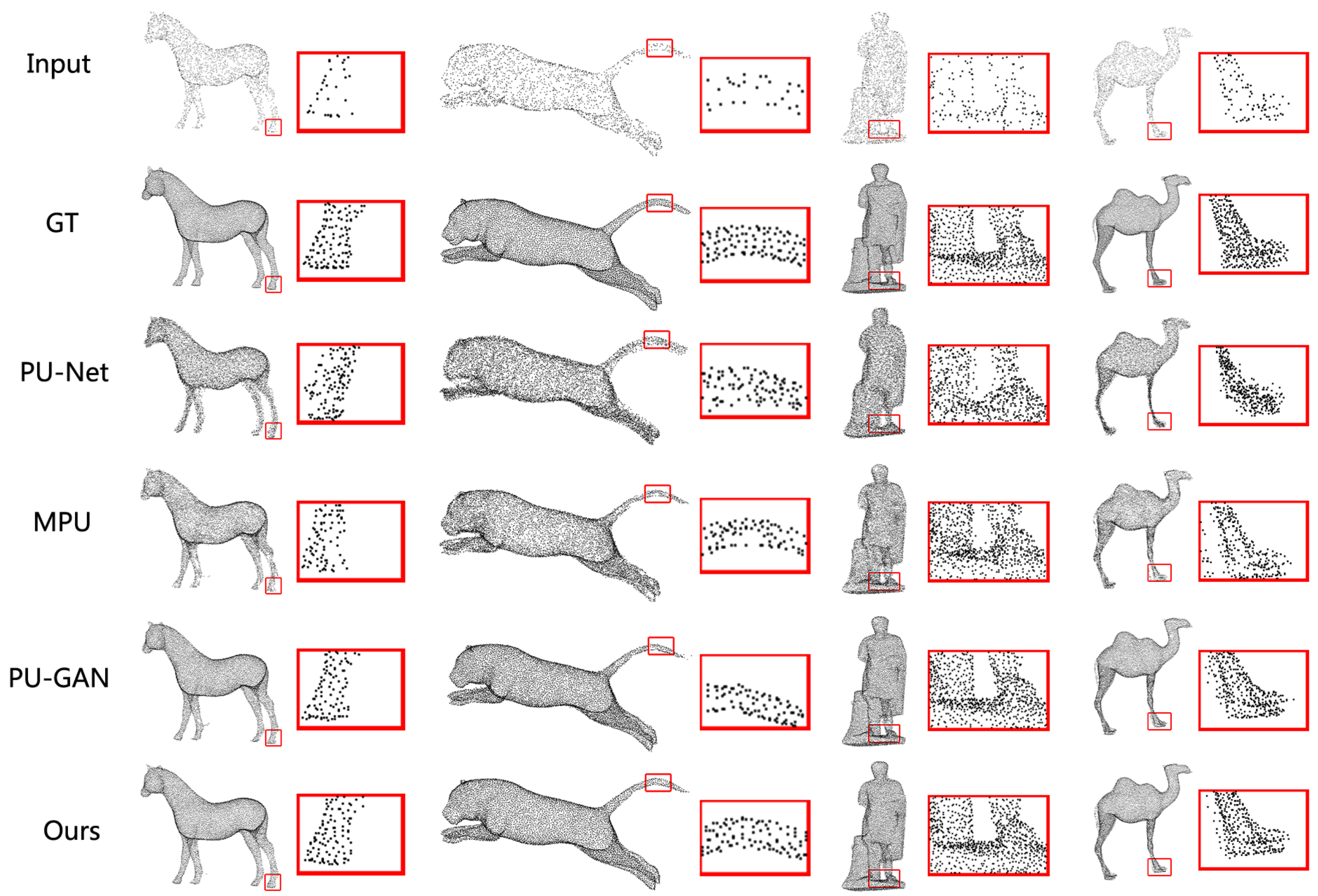

Fig. 4. Visual comparisons of upsampled point clouds (×4) by PU-Net [9], MPU [16], PU-GAN [10] and ours.

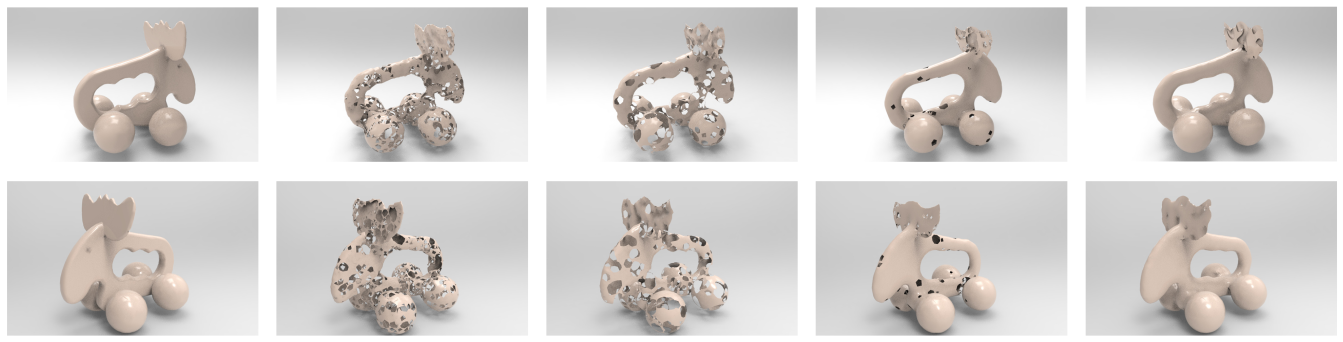

Fig. 5. Examples of synthesized images rendered by the point cloud renderer [23] from the "Elk" model, where each row corresponds to a fixed camera pose. From left to right: they are the rendered images for the GT points, upsampled points of methods PU-Net [9], MPU[16], PU-GAN[10] and Ours, respectively.

TABLE I
QUANTITATIVE COMPARISON WITH THE SOTA METHODS FOR 4×-UPSAMPLING RESULTS ON THE POINT CLOUD UPSAMPLING TASK WITHOUT NOISE AND WITH 0.5%, 1.0%, 1.5% AND 2.5% NOISE. (BOLD DENOTES THE BEST PERFORMANCE.)

Methods	level=0			level=0.5%			level=1.0%			level=1.5%			level=2.5%			#Network size	Runtime
	P2F 10^{-3}	CD 10^{-3}	HD 10^{-3}	P2F 10^{-3}	CD 10^{-3}	HD 10^{-3}	P2F 10^{-3}	CD 10^{-3}	HD 10^{-3}	P2F 10^{-3}	CD 10^{-3}	HD 10^{-3}	P2F 10^{-3}	CD 10^{-3}	HD 10^{-3}	M	s
PU-Net	8.230	0.584	6.656	5.513	0.455	5.373	9.164	0.620	7.970	13.205	0.986	10.830	21.375	1.737	21.218	10.10	**0.178**
MPU	4.288	0.480	6.033	5.233	0.613	7.060	7.958	0.695	8.329	11.371	0.922	11.240	18.676	1.420	16.555	92.50	1.807
PU-GAN	2.708	0.262	4.178	3.753	**0.311**	5.454	7.244	**0.439**	7.656	11.608	0.751	13.174	20.392	1.526	21.745	**9.57**	0.484
Ours	**2.533**	**0.259**	**3.911**	**3.613**	**0.311**	**4.955**	**4.219**	0.561	**5.481**	**8.465**	**0.574**	**8.638**	**16.568**	**1.134**	**16.056**	34.31	0.921

TABLE II
PERFORMANCE COMPARISON WITH THE SOTA APPROACHES FOR POINT CLOUD COMPLETION IN THE CD. (BOLD AND UNDERLINING DENOTE THE BEST AND SECOND PERFORMANCE, RESPECTIVELY.)

Methods	Airplane	Cabinet	Car	Chair	Lamp	Sofa	Table	Watercraft	CD (10^{-4})
Folding	12.83	23.01	14.88	25.69	21.79	21.31	20.71	11.51	19.07
PCN	9.79	22.70	12.43	25.14	22.72	20.26	20.27	11.73	18.22
PointSetVoting	6.88	21.18	15.78	22.54	18.78	28.39	19.96	11.16	18.18
AtlasNet	10.36	23.40	13.40	24.16	20.24	20.82	17.52	11.62	17.77
PointNetFCAE	10.30	19.06	11.82	24.68	20.30	20.09	17.57	10.50	16.88
TopNet	7.32	<u>18.77</u>	12.88	19.82	14.60	<u>16.29</u>	<u>14.89</u>	8.82	14.25
GRNet	<u>6.13</u>	**16.90**	**8.27**	**12.23**	**10.22**	**14.93**	**10.08**	**5.86**	**10.64**
Ours	**4.45**	20.50	<u>9.99</u>	<u>17.24</u>	<u>13.38</u>	20.70	15.27	<u>6.52</u>	<u>13.60</u>

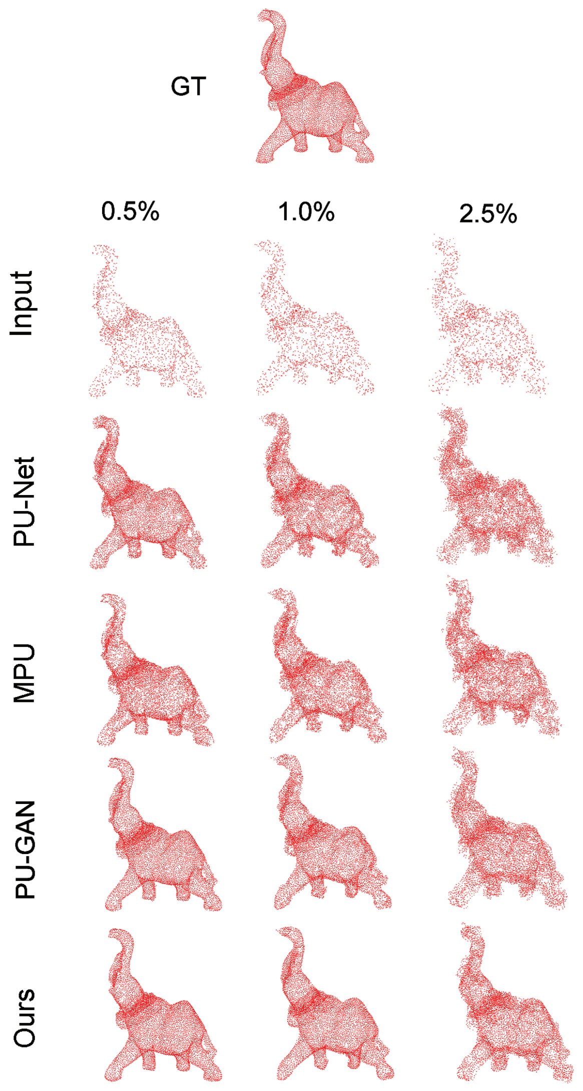

Fig. 6. The comparison of results under different noisy inputs ("Elephant"). From top to bottom: they are the GT points, input points, upsampled points of PU-Net [9], MPU [16], PU-GAN [10] and Ours. From left to right: they are the results of different models according to inputs with noisy levels of 0.5%, 1.0% and 2.5%.

keep a good shape. However, for point clouds with noise level 2.5%, the results of PU-Net, MPU and PU-GAN contain apparent outliers, *e.g.*, elephant's legs. Thus, these methods can only process point clouds with a slight noise level and not process serious noise. Compared with the SOTA methods, our proposed model is relatively robust to the noise level and can generate uniform point clouds, *e.g.*, elephant's body.

3) Point Cloud Completion: For performance evaluation on point cloud completion task, we only use one Up-UNet feature expansion module and remove the first up-feature operator in our proposed method. To protect the completion of point cloud structure, the raw incomplete point clouds is fed into the network as a whole. The training data for this task has 2048 points per 3D scene. For fast training, the number of camera poses in the point cloud render is reduced from 32 to 6. Both EMD and CD as the reconstruction loss better result than most existing models, but EMD is better than the CD from our experiment. Therefore, we employ EMD instead of CD as the reconstruction loss in the point cloud completion task. In the testing stage, we evaluate our model across 8 category from the Shapenet dataset, including "Airplane", "Cabinet", "Car", "Chair", "Lamp", "Sofa", "Table" and "Watercraft". Table II summarizes the comparison results on the leaderboard[1] provided by the official testing platform. Notably, the table shows the average result of each category, not a single 3D model. Our proposed method is better than most SOTA models for point cloud completion, but not over GRNet [64]. As shown in Fig. 7, our proposed method can protect the whole structure, even if the input points have serious distortion, *e.g.,* the car in the last row. Although our model would generate outliers in the "Chair" case, like the legs of the chair, it has a clear skeleton. The "Chair" model completed by PCN has a clear structure, but this model cannot keep the original shape. For the "Cabinet" model, even though our model has low CD values, it can get a similar structure of the GT points and good visualization. For the "Airplane" model, our model can gain more detailed information, such as the wing and head of the plane.

C. Upsampling Real-scanned Data

Our proposed method is also evaluated on real-world scanned data downloaded from KITTI dataset [1], which

[1]https://completion3d.stanford.edu/results

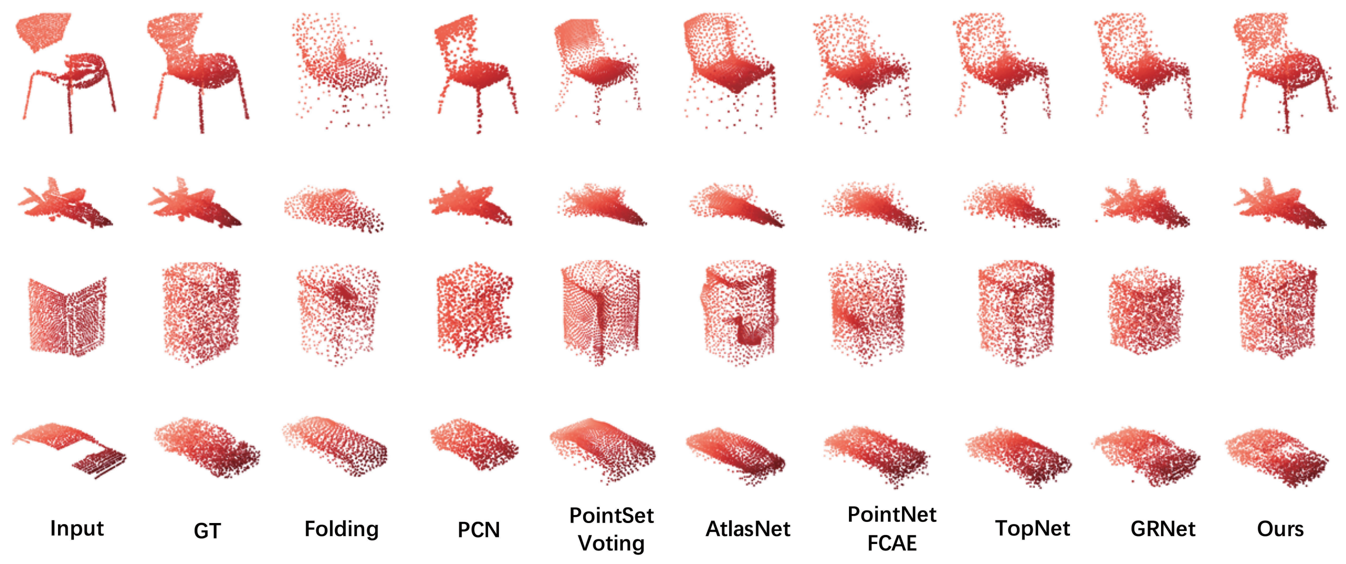

Fig. 7. Visual comparison of the results of Folding [51], PCN [30], PointSetVoting [61], AtlasNet [62], PointNetFCAE [base.], TopNet [63], GRNet [64] and our proposed method on the point cloud completion task. From top to bottom, there are the results of "Chair", "Airplane", "Cabinet" and "Car" models.

is captured by LiDAR for autonomous driving. As shown in Fig. 8, due to the limitation of hardware, the original point cloud suffers from outliers, sparsity and non-uniform distribution issues, *e.g.*, vehicles, pedestrians, and cyclists, are represented with only a few points. Due to a large amount of point cloud data from the KITTI dataset, we divide every point cloud into many patches with 256 points, upsample them 4 times separately, and finally merge them. In this manner, the point cloud becomes denser and increases more geometrical details. The dense point clouds with a good geometrical structure may benefit the other tasks, *e.g.*, point cloud segmentation and classification.

D. Ablation Study

1) Up-UNet Feature Expansion Module: To quantitatively evaluate the contribution of our proposed Up-UNet module, two deformations, including UNet-Up and Up-Down-Up, are employed to replace the Up-UNet module. Specifically, the UNet-Up module only changes the position of the first up-feature operator. The Up-Down-Up module is from PU-GAN, and it replaces the Up-UNet. The results are shown in Table III. For the UNet-Up structure, part of the point information will lose via the first two down-feature layers. Implementing an up-feature operator first can help keep the raw information. For the Up-Down-Up structure, their proposed down-feature operator does not consider the local relationship. Overall, our proposed Up-UNet module has a good performance on neighbouring feature extraction and point cloud reconstruction.

Moreover, an ablation study quantitatively evaluates the contribution of each of our proposed components, *e.g.,* the model **Ours(Up)** using the Up-feature operator instead of Up-UNet, the model **Ours(w/o CR)** without the CR module, and the model **Ours(w/o ECA)** without ECA in the upsampling layer. The model names with the signal of "#" (*e.g.,* **#Ours(Up)**, **#Ours(w/o CR)** and **#Ours(w/o ECA)**) represent that these models work for noisy point clouds. These results are from point clouds with a noise level of 2.5%. Our full pipeline performs well, and removing any component reduces the overall performance, meaning that each component contributes. In particular, removing the CR module significantly increased the difficulty of the task. Quantitative results shown in **Ours(Up)** and **#Ours(Up)** demonstrate that the Up-UNet structure plays an important role in extracting the key points and reduces noise. The model without the ECA module cannot readjust features, which leads to poor performance on the final result.

TABLE III
THE QUANTITATIVE COMPARISONS OF UP-UNET FEATURE EXPANSION MODULES AND REMOVING EACH SPECIFIC COMPONENT FROM HYBRID LOSSES.

Setting	P2F (10^{-3})	CD (10^{-3})	HD (10^{-3})
Ours(UNet-Up)	2.869	0.267	4.375
Ours(Up-Down-Up)	2.904	0.279	4.029
Ours(Up)	2.947	0.295	4.949
Ours(w/o CR)	4.740	0.421	6.401
Ours(w/o ECA)	3.696	0.342	5.953
#Ours(Up)	18.246	1.299	19.834
#Ours(w/o CR)	17.804	1.236	20.558
#Ours(w/o ECA)	17.424	1.222	18.560
#Ours	16.056	1.134	16.568
Ours (w/o $\mathcal{L}_v$)	2.552	0.260	4.298
Ours (w/o $\mathcal{L}_R$)	**2.457**	**0.253**	4.128
Ours	2.533	0.259	**3.911**

2) Hybrid Loss: To evaluate the contributions of hybrid loss on our proposed model, we remove each component of hybrid loss and evaluate the effect of it. As shown in Table III, if we do not adopt the rendering loss (denoted as **Ours (w/o $\mathcal{L}_v$)**) during the training stage, the upsampling result on the evaluation of the HD value decreases from 3.911 to 4.128.

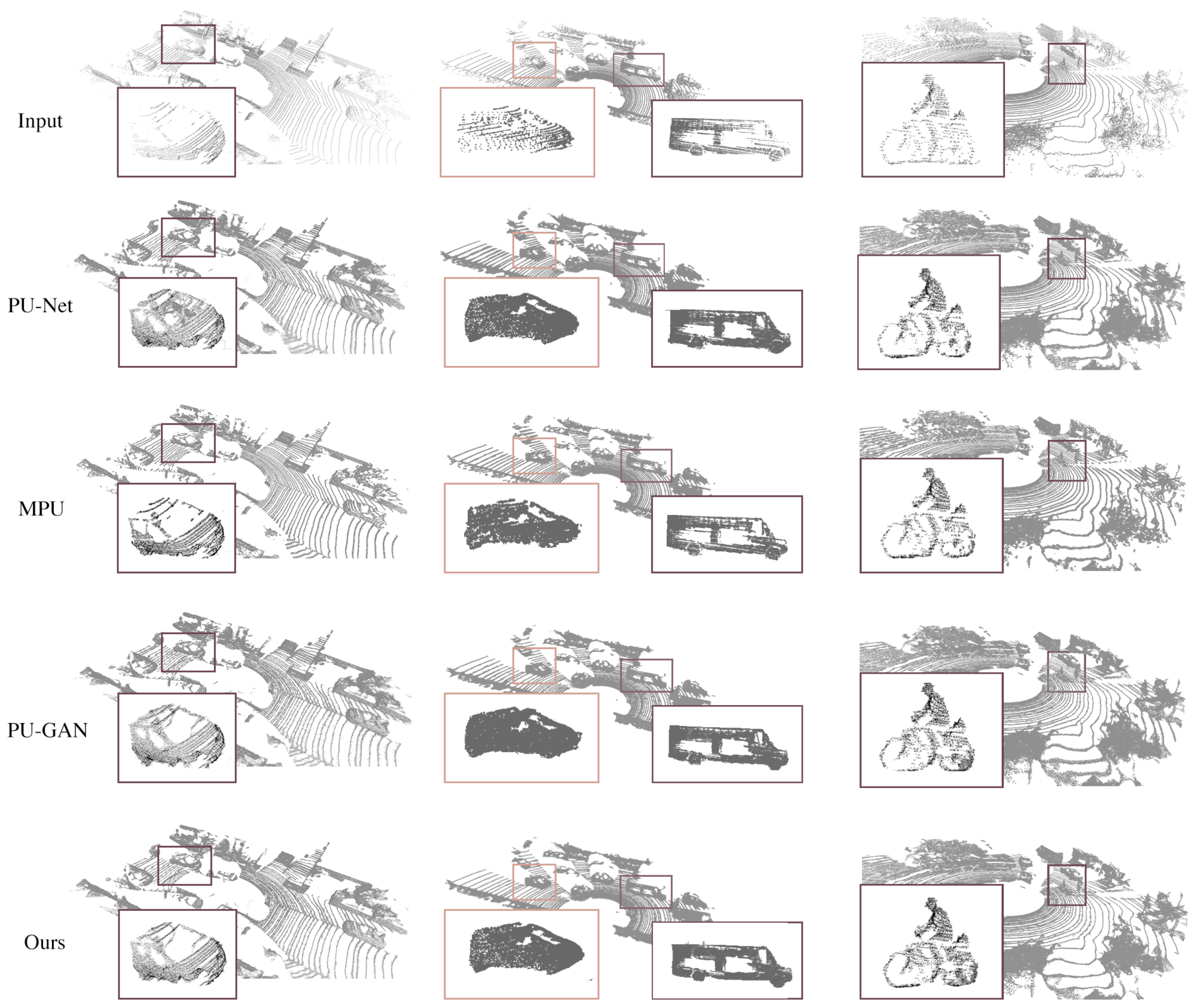

Fig. 8. Upsampling results of our proposed method on real-scanned LiDAR point clouds. We magnify some cases (*e.g.,* the vehicles, the pedestrian, and the cyclist), and our model can make point clouds denser and increase more geometrical details.

Besides quantitative results, we visualize the upsampling and Poisson surface reconstruction results in Fig. 9. The setting **Ours (w/o $\mathcal{L}_v$)** tends to produce noisy and non-uniform point sets, thus leads to more holes in the reconstructed surfaces. By contrast, our proposed method can produce more fine-grained details in the upsampled results and smoother surface, *e.g.*, tiger's leg and cow's leg.

Besides, we evaluate the setting **Ours (w/o $\mathcal{L}_R$)**, which disables the loss calculation of the first upsampling module. There is no denying that the setting **Ours (w/o $\mathcal{L}_R$)** has a better result in P2F and CD, but it can not consider the output of every iteration that introduce more artifacts reflected in Fig. 10. Since each iteration parameters are shared, this training way tries to obtain a better final output and does not consider the middle outputs. Hence, the points from the middle stages may contain some noises. To improve the quality of reconstruction after every iteration, we constrict the outputs of every iteration to have more generalization ability to upsample point clouds with various sizes, as shown in Fig. 10. Comparing with the result from the setting **Ours (w/o $\mathcal{L}_R$)**, the output point cloud of our proposed method has fewer artifacts. Due to the constraint of outputs of every stage, the model has a chance to correct the mistakes introduced in earlier stages. Besides, progressive point cloud upsampling is necessary to capture more local details because our model would adjust the scope of receptive fields according to the spatial span of the input.

V. CONCLUSIONS

In this paper, we have proposed a differentiable rendering based point cloud upsampling framework, which exploits local and global structure for progressive point cloud upsampling. Specifically, the down-feature operator of our proposed Up-UNet feature expansion module can extract key point features by removing the outliers, while the up-feature operator can expand the point features uniformly via the grid-based folding approach. With the constraint of the hybrid loss function,

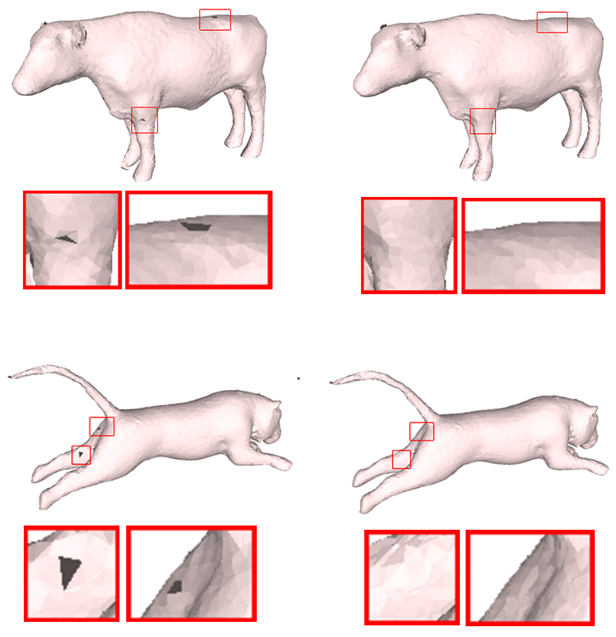

Fig. 9. The surface reconstruction of models trained without and with the rendering loss. (a) the result of the model without $\mathcal{L}_v$, and (b) the result of the model with $\mathcal{L}_v$.

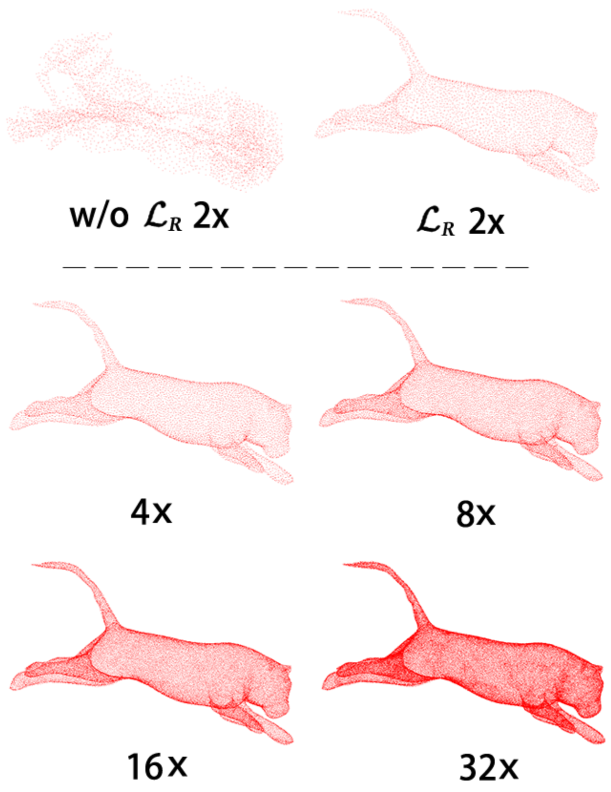

Fig. 10. Visualization of point clouds with different upsampling ratios (2×, 4×, 8×, 16× and 32×). The first point cloud is generated by the model without the middle reconstruction loss, so compared with the second point cloud, it does not have a clear structure. The rest point clouds are from the same input with different upsampling ratios. It is thus clear that our model can achieve progressive upsampling.

our proposed method can improve reconstructed point cloud data quality. Finally, we demonstrated the effectiveness of our proposed model on different tasks via extensive experiments.

References

[1] A. Geiger, P. Lenz, C. Stiller, and R. Urtasun, “Vision meets robotics: The KITTI dataset,” *The International Journal of Robotics Research*, vol. 32, no. 11, pp. 1231–1237, 2013.

[2] S. Song, S. P. Lichtenberg, and J. Xiao, “SUN RGB-D: A RGB-D scene understanding benchmark suite,” in *Proceedings of the IEEE Conference on Computer Vision and Pattern Recognition*, 2015, pp. 567–576.

[3] A. Dai, A. X. Chang, M. Savva, M. Halber, T. Funkhouser, and M. Nießner, “Scannet: Richly-annotated 3D reconstructions of indoor scenes,” in *Proceedings of the IEEE Conference on Computer Vision and Pattern Recognition*, 2017, pp. 5828–5839.

[4] R. Mekuria, K. Blom, and P. Cesar, “Design, implementation, and evaluation of a point cloud codec for tele-immersive video,” *IEEE Transactions on Circuits and Systems for Video Technology*, vol. 27, no. 4, pp. 828–842, 2016.

[5] H. Zhou, K. Chen, W. Zhang, H. Fang, W. Zhou, and N. Yu, “DUP-Net: Denoiser and upsampler network for 3D adversarial point clouds defense,” in *Proceedings of the IEEE International Conference on Computer Vision*, 2019, pp. 1961–1970.

[6] X. Wang, J. He, and L. Ma, “Exploiting local and global structure for point cloud semantic segmentation with contextual point representations,” in *Advances in Neural Information Processing Systems*, 2019, pp. 4573–4583.

[7] P. Achlioptas, O. Diamanti, I. Mitliagkas, and L. Guibas, “Learning representations and generative models for 3D point clouds,” in *International Conference on Machine Learning*, 2018, pp. 40–49.

[8] X. Huang, J. Zhang, Q. Wu, L. Fan, and C. Yuan, “A Coarse-to-Fine algorithm for matching and registration in 3D cross-source point clouds,” *IEEE Transactions on Circuits and Systems for Video Technology*, vol. 28, no. 10, pp. 2965–2977, 2018.

[9] L. Yu, X. Li, C.-W. Fu, D. Cohen-Or, and P.-A. Heng, “PU-Net: Point cloud upsampling network,” in *Proceedings of the IEEE Conference on Computer Vision and Pattern Recognition*, 2018, pp. 2790–2799.

[10] R. Li, X. Li, C.-W. Fu, D. Cohen-Or, and P.-A. Heng, “PU-GAN: A point cloud upsampling adversarial network,” in *IEEE International Conference on Computer Vision*, 2019, pp. 7203–7212.

[11] Y. Qian, J. Hou, S. Kwong, and Y. He, “PUGeo-Net: A geometry-centric network for 3D point cloud upsampling,” *Proceedings of the European Conference on Computer Vision*, pp. 752–769, 2020.

[12] Y. Zhang, X. Tuo, Y. Huang, and J. Yang, “A tv forward-looking super-resolution imaging method based on tsvd strategy for scanning radar,” *IEEE Transactions on Geoscience and Remote Sensing*, vol. 58, no. 7, pp. 4517–4528, 2020.

[13] H. Huang, D. Li, H. Zhang, U. Ascher, and D. Cohen-Or, “Consolidation of unorganized point clouds for surface reconstruction,” *ACM Transactions on Graphics*, vol. 28, no. 5, pp. 1–7, 2009.

[14] M. Berger, A. Tagliasacchi, L. M. Seversky, P. Alliez, G. Guennebaud, J. A. Levine, A. Sharf, and C. T. Silva, “A survey of surface reconstruction from point clouds,” in *Computer Graphics Forum*, vol. 36, no. 1, 2017, pp. 301–329.

[15] H. Hoppe, T. DeRose, T. Duchamp, J. McDonald, and W. Stuetzle, “Surface reconstruction from unorganized points,” in *Proceedings of the 19th Annual Conference on Computer Graphics and Interactive Techniques*, 1992, pp. 71–78.

[16] Y. Wang, S. Wu, H. Huang, D. Cohen-Or, and O. Sorkine-Hornung, “Patch-based progressive 3D point set upsampling,” in *Proceedings of the IEEE Conference on Computer Vision and Pattern Recognition*, 2019, pp. 5958–5967.

[17] G. Qian, A. Abualshour, G. Li, A. Thabet, and B. Ghanem, “PU-GCN: Point Cloud Upsampling using Graph Convolutional Networks,” in *Proceedings of the IEEE/CVF Conference on Computer Vision and Pattern Recognition*, 2021.

[18] S. Ye, D. Chen, S. Han, Z. Wan, and J. Liao, “Meta-pu: An arbitrary-scale upsampling network for point cloud,” *IEEE Transactions on Visualization and Computer Graphics*, 2021.

[19] R. A. Newcombe, S. Izadi, O. Hilliges, D. Molyneaux, D. Kim, A. J. Davison, P. Kohi, J. Shotton, S. Hodges, and A. Fitzgibbon, “KinectFusion: Real-time dense surface mapping and tracking,” in *2011 10th IEEE International Symposium on Mixed and Augmented Reality*, 2011, pp. 127–136.

[20] A. Tagliasacchi, H. Zhang, and D. Cohen-Or, "Curve skeleton extraction from incomplete point cloud," in *ACM SIGGRAPH 2009 papers*, 2009, pp. 1–9.

[21] R. Schnabel, R. Wahl, and R. Klein, "Efficient RANSAC for point-cloud shape detection," in *Computer Graphics Forum*, vol. 26, no. 2, 2007, pp. 214–226.

[22] C. R. Qi, L. Yi, H. Su, and L. J. Guibas, "PointNet++: Deep hierarchical feature learning on point sets in a metric space," in *Advances in Neural Information Processing Systems*, 2017, pp. 5099–5108.

[23] E. Insafutdinov and A. Dosovitskiy, "Unsupervised learning of shape and pose with differentiable point clouds," in *Advances in Neural Information Processing Systems*, 2018, pp. 2802–2812.

[24] M. Alexa, J. Behr, D. Cohen-Or, S. Fleishman, D. Levin, and C. T. Silva, "Computing and rendering point set surfaces," *IEEE Transactions on Visualization and Computer Graphics*, vol. 9, no. 1, pp. 3–15, 2003.

[25] Y. Lipman, D. Cohen-Or, D. Levin, and H. Tal-Ezer, "Parameterization-free projection for geometry reconstruction," *ACM Transactions on Graphics*, vol. 26, no. 3, pp. 22–es, 2007.

[26] L. Yu, X. Li, C.-W. Fu, D. Cohen-Or, and P.-A. Heng, "EC-Net: An edge-aware point set consolidation network," in *Proceedings of the European Conference on Computer Vision*, 2018, pp. 386–402.

[27] J. Lin, X. Shi, Y. Gao, K. Chen, and K. Jia, "Cad-pu: A curvature-adaptive deep learning solution for point set upsampling," *arXiv preprint arXiv:2009.04660*, 2020.

[28] H. Son and Y. M. Kim, "Saum: Symmetry-aware upsampling module for consistent point cloud completion," in *Proceedings of the Asian Conference on Computer Vision*, 2020.

[29] Z. Huang, Y. Yu, J. Xu, F. Ni, and X. Le, "PF-Net: Point fractal network for 3D point cloud completion," in *Proceedings of the IEEE/CVF Conference on Computer Vision and Pattern Recognition*, 2020, pp. 7662–7670.

[30] W. Yuan, T. Khot, D. Held, C. Mertz, and M. Hebert, "PCN: Point completion network," in *2018 International Conference on 3D Vision*, 2018, pp. 728–737.

[31] L. Pan, "ECG: Edge-aware point cloud completion with graph convolution," *IEEE Robotics and Automation Letters*, vol. 5, no. 3, pp. 4392–4398, 2020.

[32] X. Wang, M. H. Ang Jr, and G. H. Lee, "Cascaded refinement network for point cloud completion," in *Proceedings of the IEEE/CVF Conference on Computer Vision and Pattern Recognition*, 2020, pp. 790–799.

[33] K. He, X. Zhang, S. Ren, and J. Sun, "Deep residual learning for image recognition," in *Proceedings of the IEEE Conference on Computer Vision and Pattern Recognition*, 2016, pp. 770–778.

[34] G. Huang, Z. Liu, L. Van Der Maaten, and K. Q. Weinberger, "Densely connected convolutional networks," in *Proceedings of the IEEE Conference on Computer Vision and Pattern Recognition*, 2017, pp. 4700–4708.

[35] O. Ronneberger, P. Fischer, and T. Brox, "U-Net: Convolutional networks for biomedical image segmentation," in *International Conference on Medical Image Computing and Computer-assisted Intervention*, 2015, pp. 234–241.

[36] C. R. Qi, H. Su, K. Mo, and L. J. Guibas, "Pointnet: Deep learning on point sets for 3D classification and segmentation," in *Proceedings of the IEEE Conference on Computer Vision and Pattern Recognition*, 2017, pp. 652–660.

[37] M. M. Loper and M. J. Black, "OpenDR: An approximate differentiable renderer," in *European Conference on Computer Vision*, 2014, pp. 154–169.

[38] H. Kato, Y. Ushiku, and T. Harada, "Neural 3D mesh renderer," in *Proceedings of the IEEE Conference on Computer Vision and Pattern Recognition*, 2018, pp. 3907–3916.

[39] T.-M. Li, M. Aittala, F. Durand, and J. Lehtinen, "Differentiable monte carlo ray tracing through edge sampling," *ACM Transactions on Graphics*, vol. 37, no. 6, pp. 1–11, 2018.

[40] W. Yifan, F. Serena, S. Wu, C. Öztireli, and O. Sorkine-Hornung, "Differentiable surface splatting for point-based geometry processing," *ACM Transactions on Graphics*, vol. 38, no. 6, pp. 1–14, 2019.

[41] S. Liu, T. Li, W. Chen, and H. Li, "Soft Rasterizer: A differentiable renderer for image-based 3D reasoning," in *Proceedings of the IEEE International Conference on Computer Vision*, 2019, pp. 7708–7717.

[42] C.-H. Lin, C. Kong, and S. Lucey, "Learning efficient point cloud generation for dense 3D object reconstruction," *arXiv preprint arXiv:1706.07036*, 2017.

[43] R. Roveri, A. C. Öztireli, I. Pandele, and M. Gross, "PointProNets: Consolidation of point clouds with convolutional neural networks," in *Computer Graphics Forum*, vol. 37, no. 2, 2018, pp. 87–99.

[44] G. Liu, D. Ceylan, E. Yumer, J. Yang, and J.-M. Lien, "Material editing using a physically based rendering network," in *Proceedings of the IEEE International Conference on Computer Vision*, 2017, pp. 2261–2269.

[45] T. H. Nguyen-Phuoc, C. Li, S. Balaban, and Y. Yang, "RenderNet: A deep convolutional network for differentiable rendering from 3D shapes," in *Advances in Neural Information Processing Systems*, 2018, pp. 7891–7901.

[46] S. Tulsiani, T. Zhou, A. A. Efros, and J. Malik, "Multi-view supervision for single-view reconstruction via differentiable ray consistency," in *Proceedings of the IEEE conference on Computer Vision and Pattern Recognition*, 2017, pp. 2626–2634.

[47] P. Hermosilla, T. Ritschel, P.-P. Vázquez, À. Vinacua, and T. Ropinski, "Monte carlo convolution for learning on non-uniformly sampled point clouds," *ACM Transactions on Graphics*, vol. 37, no. 6, pp. 1–12, 2018.

[48] H.-T. D. Liu, M. Tao, and A. Jacobson, "Paparazzi: surface editing by way of multi-view image processing." *ACM Trans. Graph.*, vol. 37, no. 6, pp. 221–1, 2018.

[49] V. Sitzmann, M. Zollhöfer, and G. Wetzstein, "Scene representation networks: Continuous 3D-structure-aware neural scene representations," in *Advances in Neural Information Processing Systems*, 2019, pp. 1121–1132.

[50] B. Mildenhall, P. P. Srinivasan, M. Tancik, J. T. Barron, R. Ramamoorthi, and R. Ng, "NeRF: Representing scenes as neural radiance fields for view synthesis," in *Proceedings of the European Conference on Computer Vision*, 2020, pp. 405–421.

[51] Y. Yang, C. Feng, Y. Shen, and D. Tian, "Foldingnet: Point cloud auto-encoder via deep grid deformation," in *Proceedings of the IEEE Conference on Computer Vision and Pattern Recognition*, 2018, pp. 206–215.

[52] Q. Wang, B. Wu, P. Zhu, P. Li, W. Zuo, and Q. Hu, "ECA-Net: Efficient channel attention for deep convolutional neural networks," in *Proceedings of the IEEE/CVF Conference on Computer Vision and Pattern Recognition*, 2020, pp. 11 534–11 542.

[53] X. Wang, R. Girshick, A. Gupta, and K. He, "Non-local neural networks," in *Proceedings of the IEEE Conference on Computer Vision and Pattern Recognition*, 2018, pp. 7794–7803.

[54] J. Hu, L. Shen, and G. Sun, "Squeeze-and-excitation networks," in *Proceedings of the IEEE Conference on Computer Vision and Pattern Recognition*, 2018, pp. 7132–7141.

[55] S. Woo, J. Park, J.-Y. Lee, and I. So Kweon, "Cbam: Convolutional block attention module," in *Proceedings of the European Conference on Computer Vision*, 2018, pp. 3–19.

[56] H. Fan, H. Su, and L. J. Guibas, "A point set generation network for 3D object reconstruction from a single image," in *Proceedings of the IEEE Conference on Computer Vision and Pattern Recognition*, 2017, pp. 605–613.

[57] "Visionair," [Online; accessed on 14-November-2017].

[58] A. X. Chang, T. Funkhouser, L. Guibas, P. Hanrahan, Q. Huang, Z. Li, S. Savarese, M. Savva, S. Song, H. Su, *et al.*, "ShapeNet: An information-rich 3D model repository," *arXiv preprint arXiv:1512.03012*, 2015.

[59] D. P. Kingma and J. Ba, "Adam: A method for stochastic optimization," in *3rd International Conference on Learning Representations*, 2015.

[60] M. Berger, J. A. Levine, L. G. Nonato, G. Taubin, and C. T. Silva, "A benchmark for surface reconstruction," *ACM Transactions on Graphics*, vol. 32, no. 2, pp. 1–17, 2013.

[61] J. Zhang, W. Chen, Y. Wang, R. Vasudevan, and M. Johnson-Roberson, "Point set voting for partial point cloud analysis," *IEEE Robotics and Automation Letters*, vol. 6, no. 2, pp. 596–603, 2021.

[62] T. Groueix, M. Fisher, V. G. Kim, B. C. Russell, and M. Aubry, "A papier-mâché approach to learning 3d surface generation," in *Proceedings of the IEEE Conference on Computer Vision and Pattern Recognition*, June 2018.

[63] L. P. Tchapmi, V. Kosaraju, H. Rezatofighi, I. Reid, and S. Savarese, "Topnet: Structural point cloud decoder," in *Proceedings of the IEEE Conference on Computer Vision and Pattern Recognition*, 2019, pp. 383–392.

[64] H. Xie, H. Yao, S. Zhou, J. Mao, S. Zhang, and W. Sun, "GRNet: Gridding residual network for dense point cloud completion," in *Proceedings of the European Conference on Computer Vision*, 2020, pp. 365–381.